Magnetothermal Oscillations in Dilute Aluminum-Magnesium Alloys*

J. C. ABELE† AND F. J. BLATT
Michigan State University, East Lansing, Michigan 48823
(Received 28 July 1969)

The magnetothermal oscillation (MTO) technique has been employed to study the effect of alloying aluminum with magnesium. Changes in the third-band electron Fermi surface as well as the Dingle temperatures associated with electron scattering have been measured in samples containing up to 0.4 at. % magnesium. Angular regions where the signal was of sufficient amplitude and reasonably free of heating indicate that the simple rigid-band model is applicable. Techniques which render the MTO experiment especially well suited to Dingle-temperature measurements are presented.

I. INTRODUCTION

MUCH progress has been made during the past decade in our understanding of the electronic structure of pure metals. The most detailed information has come from de Haas–van Alphen studies or experiments of a similar kind (Shubnikov–de Haas oscillations, magnetothermal oscillations, magnetoacoustic resonance) that measure the extremal cross-section areas or caliper dimensions of the Fermi surface.[1] These techniques impose fairly stringent requirements on sample purity and temperature, since good signals are obtained only if the conditions $\omega_c\tau>1$ and $\hbar\omega_c>kT$ are satisfied, where ω_c is the cyclotron frequency and τ is the relaxation time of the electrons participating in the oscillatory phenomenon.

Studies of the electronic structure of alloys using these methods are limited by the above-mentioned requirements to relatively dilute systems or ordered alloys, i.e., intermetallic compounds. Nevertheless, considerable effort has in recent years been devoted to alloys in an attempt to elucidate their electronic structure and, in particular, determine to what extent simple models, such as the rigid-band model (RBM), may be applicable.

The electronic structure of dilute aluminum-base alloys using the de Haas–van Alphen techniques has been investigated recently by Shepherd and Gordon (SG).[2] SG used the solutes Ag, Mg, Zn, Si, and Ge, but experienced some difficulty in growing satisfactory single-crystal samples of Al-Mg and reported data on only one sample. Our results on several Al-Mg samples thus complement theirs, provide further support of the RBM in the dilute concentration region, and, incidentally, shed additional light on the interpretation of data obtained by the method of magnetothermal oscillations (MTO).

In view of the excellent background information on alloy studies, including an up-to-data bibliography, presented by SG, we shall not dwell on this matter further, but refer the reader to that article.

II. MAGNETOTHERMAL OSCILLATIONS

The theoretical treatment of magnetothermal oscillations, a technique first employed by Kunzler *et al.*,[3] is in many respects analogous to that of the de Haas–van Alphen effect. According to Lifshitz and Kosevitch,[4] the oscillatory part of the free energy of the electron system, assuming a single closed sheet of Fermi surface, is given by

$$F_{\rm osc}=kTH^{3/2}\sum_{l=1}^{\infty}A_l\frac{\cos(2\pi f_l/H+\varphi_l)}{\sinh(b_lT/H)}e^{-b_lX_D/H}, \quad (1)$$

where

$$A_l=2\left[\cos\left(\frac{l\pi gm_c^*}{2m}\right)\right]\left(\frac{e}{\hbar c}\right)^{3/2}\Big/\left|\frac{\partial^2\mathbf{A}_o}{\partial k_z^{\,2}}\right|_{E_F}^{1/2}l^{3/2}, \quad (2)$$

$$b_l=(1.47\times10^5)lm_c^*/m, \quad \mathrm{G/^\circ K},$$

$$f_l=l(\hbar c/2\pi e)\mathbf{A}_o(E_F)=lf,$$

$$\varphi_l=-2\pi l\gamma\mp\tfrac{1}{4}\pi,$$

$$X_D=\hbar/2\pi k\tau.$$

Here, γ is a phase factor equal to $\frac{1}{2}$ for a quadratic dispersion law, τ is the Brailsford lifetime of an orbital state ($\tau=\frac{1}{2}\tau_{\rm Dingle}$), $\mathbf{A}_o$ is an extremal cross-section area of the Fermi surface in a plane perpendicular to the field H which defines the z direction, and the other constants have their usual significance.

In a de Hass–van Alphen experiment one observes, in effect, the oscillatory part of the magnetization

$$M_{\rm osc}=-\left(\frac{\partial F}{\partial H}\right)_T=\sum_l M_{\rm osc}{}^{(l)}, \quad (3)$$

where

$$M_{\rm osc}{}^{(l)}=-A_lT\frac{2\pi f}{H^{1/2}}\frac{\sin(2\pi fl/H+\varphi_l)}{(\sinh b_lT/H)}e^{-b_lX_D/H}. \quad (4)$$

* This work supported in part by a grant from the National Science Foundation.
† Presently at the Douglas Advanced Research Laboratories, Huntington Beach, Calif.
[1] *Solid State Physics*, edited by J. F. Cochran and R. R. Haering (Gordon and Breach, Science Publishers, Inc., New York, 1968), Vol. I.
[2] J. P. G. Shepherd and W. L. Gordon, Phys. Rev. 169, 541 (1968).
[3] J. E. Kunzler, F. S. L. Hsu, and W. S. Boyle, Phys. Rev. 128, 1084 (1962).
[4] I. M. Lifshitz and A. Kosevitch, Zh. Eksperim. i Teor. Fiz. 29, 730 (1955) [English transl.: Soviet Phys.—JETP 2, 172 (1956)].

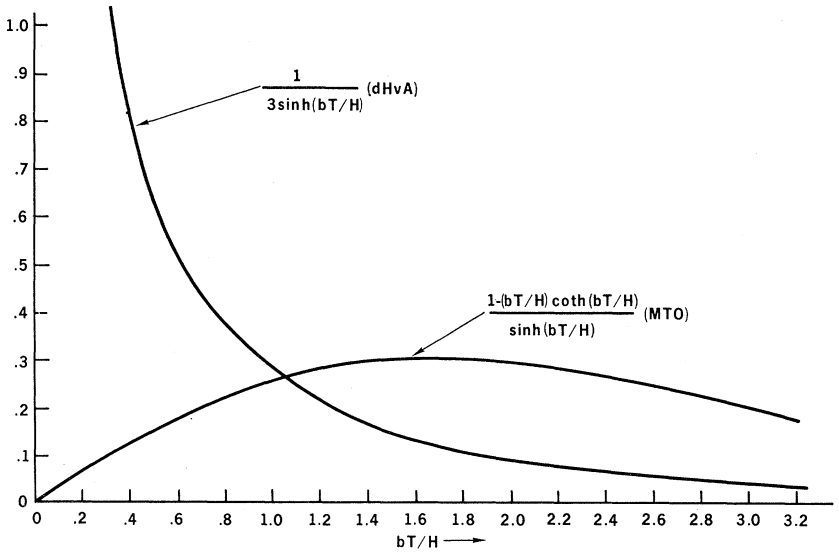

FIG. 1. The hyperbolic dependence of the amplitude of the dHvA and MTO effects upon the parameter $bT/H=1.47\times10^5\, m_c^*/m$ G/°K.

In arriving at Eq. (4) all the derivatives with respect to H, except that of the rapidly varying trigonometric function of Eq. (1), have been neglected.

In the idealized adiabatic MTO experiment, the crystal is maintained in perfect thermal isolation and its temperature is measured as the magnetic field is varied. Elementary thermodynamic arguments lead to

$$\delta T_{\rm osc}=\frac{TH^{3/2}}{C_H}\sum_l A_l\cos\left(\frac{2\pi fl}{H}+\varphi_l\right)\times\left[\frac{1-(b_lT/H)\coth(b_lT/H)}{\sinh(b_lT/H)}\right]e^{-b_lX_D/H}, \quad (5)$$

where $\delta T_{\rm osc}$ is the oscillatory departure of the temperature from that at $H=0$, and C_H is the crystal's specific heat at constant magnetic field. Although C_H also has an oscillatory component, it is sufficiently small compared with the field-independent term to be negligible in these experiments.

While the two methods (de Haas–van Alphen and MTO) for studying the Fermi surface yield essentially the same information, such as extremal cross sections, there are some significant practical differences arising from the different dependences of the oscillation amplitudes on field and temperature, and the relative contributions of higher harmonics, especially at low temperatures.

Turning first to the matter of harmonic content, expansion of the hyperbolic functions for the case $b_lT/H<1$ shows that, whereas $M_{\rm osc}^{(l)}/M_{\rm osc}^{(1)}=l^{-3/2}$, the corresponding ratio $\delta T_{\rm osc}^{(l)}/\delta T_{\rm osc}^{(1)}=l^{-1/2}$. Thus, in MTO experiments at low temperature or high fields the harmonic content of the oscillatory pattern is much greater than in de Haas–van Alphen experiments. The same is also true for thermopower[5] and Peltier oscillations.[6] The resulting distinctive asymmetry can be of value in determining the form of extremal surface (electron or holelike) which gives rise to the observed oscillations. Moreover, the study of higher harmonics, particularly their orientation dependence, could also be employed in a determination of the g factor. The current practice in g-factor studies is to search for directions along which the factor $\cos(l\pi gm_c^*/2m)$ vanishes for $l=1$.[7] If m_c^* is known from other experimental data (temperature dependence of the amplitude) the g factor can then be ascertained. A search for directions along which higher harmonics ($l=2, 3, \ldots$) vanish could allow a more complete mapping of the g factor over the Fermi surface than has heretofore been possible.

The difference between the corresponding amplitude factor for the de Haas–van Alphen and MTO signals over a wide range of the variable b_lT/H is shown in Fig. 1. From Fig. 1 it is obvious that over a substantial range of magnetic field centered about $H\simeq0.67b_lT$ this amplitude factor is essentially independent of field. Consequently, the amplitude of $\delta T_{\rm osc}$ at a given temperature within this range of H varies as $H^{3/2}\exp(-b_lX_D/H)$. Herein lies one of the main advantages of the MTO technique, particularly in studies of dilute alloys, since it permits a straightforward separation of damping due to the actual temperature T and that due to the Dingle temperature X_D.

This advantageous field dependence is, however, not without its drawbacks. Because of the relatively weak dependence of the MTO amplitude on b_lT/H the technique is not well suited to measurements of m_c^*. The method we have employed is to measure the amplitude at a given field as a function of temperature. These amplitudes are then independent of $H^{3/2}\exp(-b_lX_D/H)$

[5] J. A. Woollam and P. A. Schroeder, Phys. Rev. Letters **21**, 81 (1968).

[6] H. J. Trodahl and F. J. Blatt, Phys. Rev. **180**, 706 (1969).

[7] J. B. Ketterson and L. R. Windmiller, Phys. Rev. Letters **20**, 321 (1968).

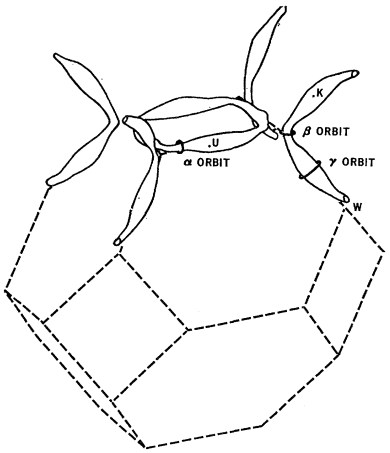

FIG. 2. Ashcroft's 4 OPW pseudopotential model for the third-band electron Fermi surface of aluminum.

and can be fit to the amplitude function shown in Fig. 1 using only two parameters, m_c^* and a scale factor. In particular, for a given field value the temperature, at which the amplitude attains its maximum, depends only on m_c^*/m and a combination of fundamental constants. Here, too, the high harmonic content of MTO signals can play a significant role and, if ignored, the results may suggest an anomalous field dependence of m_c^*/m. We shall return to this point later.

III. EXPERIMENTAL PROCEDURE

A. Sample Preparation

The sample of pure aluminum was spark-cut from a 99.999%-pure Al single crystal purchased from Metals Research, Ltd. The alloys were prepared from 99.9998%-pure Al and 99.99%-pure Mg purchased from Cominco and Jarrel-Ash Co., respectively. Appropriate quantities of Al and Mg were melted together in an induction furnace and chill cast into an aluminum mold. Each ingot was poured twice, and the procedure was performed in a reduced nitrogen atmosphere. The alloy ingots prepared in this manner were then zone leveled under an elliptical heat lamp at a pass rate of 1.5 cm/h. A second, reverse pass was used to assure uniformity over the central region. The optical method has the advantage that one can easily monitor the molten zone during the leveling procedure. Generally, at the end of this process the ingot was either a single crystal or consisted of a few large single-crystal segments.

The central region was then cut out and Laue back-reflection photographs were taken to establish that the sample was indeed a single crystal and to ascertain its orientation. After the sample orientation had been established, it was planed in a {100} plane and mounted on a small graphite support. The support with the sample firmly attached to it could then be mounted in a rotable sample holder at an orientation initially known to within $\pm 2°$. Final alignment was made using the oscillatory pattern during magnet rotations.

Prior to mounting, the samples, whose typical shape was a pillbox about 8 mm in diam and 6 mm in height, were weighed and the Mg concentration determined from residual-resistance-ratio measurements. After completion of the experiment, the samples were cut into three segments and sent to Schwartzkopf Analytical Laboratory for analysis; these showed Mg concentrations in good agreement with the residual-resistance results and no observable concentration gradients.

B. Measurement Technique

A carbon resistor served as the temperature sensor. The resistor was prepared from a $\frac{1}{8}$-W 47-Ω Ohmite resistor. Two sides were ground flat and the resistor glued to the sample using G.E. 7031 varnish with a thin piece of cigarette paper providing electrical insulation. A second resistor was similarly prepared and glued to the lower plate of the sample rotator, which was in intimate contact with the helium bath. These two resistors constituted two arms of an ac Wheatstone bridge, and the bridge unbalance, observed with a phase-sensitive detector, provided a measure of the sample temperature relative to that of the cryogenic bath.

Since during field sweeps and field rotations the sample heats by virtue of induced eddy currents, some heat leak between the sample and the cryogenic bath had to be provided. This heat leak consisted of a short length of No. 40–No. 46 commerical copper wire glued to the sample and soldered to the lower plate of the sample rotator. Typical thermal time constants were 2–5 sec.

The effect of this incomplete thermal isolation of the sample upon Eq. (5) is to multiply each term of the sum by the factor

$$B_T=[1+(\tau_{\rm osc}/2\pi\tau_Q)^2]^{-1/2}$$

and introduce a phase shift of $\frac{1}{2}\pi-\tan^{-1}(2\pi\tau_Q/\tau_{\rm osc})$ in the oscillatory trigonometric term. Here, the thermal time constant $\tau_Q=C_H/K$, where K is the thermal conductance of the heat leak.

Since we were interested in measuring absolute as well as relative amplitudes of $\delta T_{\rm osc}$, we needed to know τ_Q. This time constant was measured by determining the equilibrium temperature of the crystal when a known amount of heat was supplied to it by means of a calibrated heater glued to it. Time constants were measured at several temperatures and for magnetic fields between 10 and 21 kG. The field variation of τ_Q over this range was about 3%.

If the field is swept linearly with time, $\tau_{\rm osc}$ increases with increasing H, and thus the theoretical field dependence of the amplitude of $\delta T_{\rm osc}$ as given by Eq. (5) is further modified by the field dependence of B_T. To obviate this additional complication it is desirable to use a sweep rate such that $1/H$ is proportional to time.

A simple electronic control circuit which accomplishes this function is described in the Appendix. A $1/H$ sweep has the further obvious advantage that it allows the use of filtering techniques which aid in the detection of low-amplitude oscillations.

An advantageous feature of the heat leak is that it serves as a low-frequency attenuator. Thus, by adjusting the sweep rate, low-frequency oscillations can be damped out and high-frequency components made more prominent. This feature may also impart to the signals an anomalously large harmonic content. Hence, in studying harmonic distortion of signals, the sweep rate must be maintained high enough so that $\tau_{\rm osc} < 2\pi\tau_Q$ or else the term B_T must be taken into account.

The magnetic field was measured using an NMR calibrated hall probe, and plotted simultaneously with the thermal oscillations on a two-pen strip-chart recorder.

IV. RESULTS AND DISCUSSION

A. Pure Aluminum

Working at fields up to 22 kG and at temperatures between 1.1 and 4.2°K, we observed MTO signals with frequencies varying between 2.5 and 50×10^5 G. These frequencies have all been measured previously by several investigators[8] and been attributed to extremal orbits associated with the third-zone electron surface as calculated by Ashcroft.[9] The Ashcroft model is shown in Fig. 2 using the notation introduced in Ref. 8. Oscillations corresponding to the α, β, and γ orbits are readily detected with the MTO technique, although their resolution becomes difficult at orientations where oscillations from many different orbits contribute to the signal.

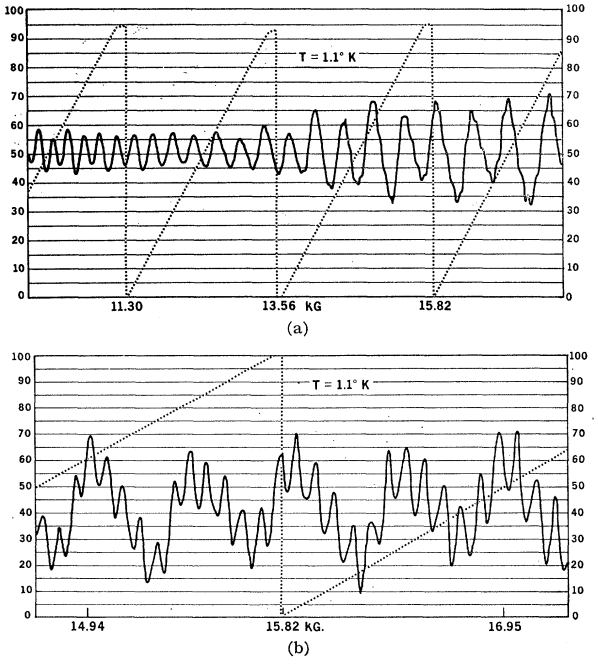

FIG. 3. The high-pass thermal filter. (a) Low-frequency data with a sweep rate of 700 G/min. (b) Higher-frequency data with a sweep rate of 230 G/min. The higher-frequency oscillations apparent at higher field in (a) become the dominant oscillations in (b) using only the thermal filtering technique.

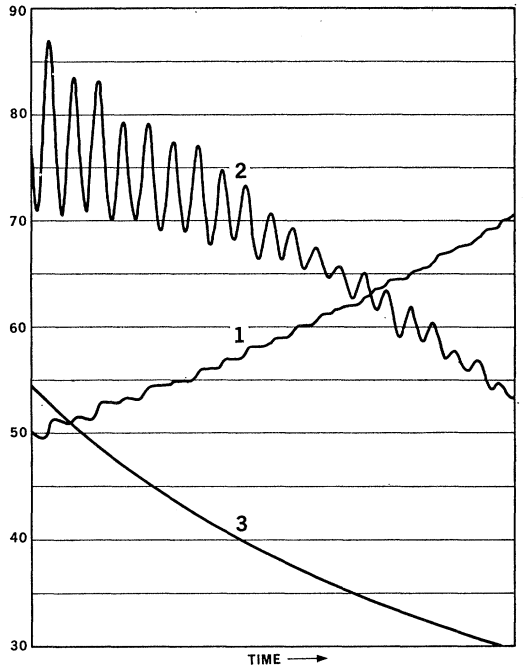

FIG. 4. Magnetothermal oscillations using the $1/H$ sweep described in the Appendix. Curve 1 is the unfiltered signal. Curve 2 is the result of filtering using a tunable bridge-tee active filter. Curve 3 is a trace proportional to the magnetic field.

To sort out the various frequencies, several techniques were employed. The effective thermal high-pass filter B_T in our version of the MTO technique was used to separate the higher-frequency γ oscillations from the α and β oscillations. An example of the method is shown in Figs. 3(a) and 3(b), which show the same region in H but surveyed at two different sweep rates. In cases where a higher Q was desirable, we used the $1/H$ sweep with either wide-band integrator-differentiator or narrower-band bridge-tee active filters. An example of the usefulness of this combination for recovery of a poorly resolved alloy signal is given in Fig. 4.

For steady-field rotations in the {100} plane, the oscillations from the central region of the arms predominated. The rotation patterns could, in this case, be interpreted simply, and the angular variation of the extremal cross section of the arm determined. To make an empirical estimate of the $|\partial^2\mathbf{A}/\partial k_z^2|^{-1/2}$ factor in Eq. (2), we have employed the following scheme.

Consider a piece of Fermi surface having roughly cylindrical symmetry about an axis determined by the

[8] C. O. Larson and W. L. Gordon, Phys. Rev. **156**, 703 (1967).

[9] N. W. Ashcroft, Phil. Mag. **8**, 2055 (1963).

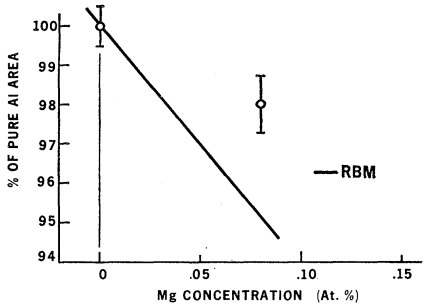

FIG. 5. Changes in the α cross section for the $\langle 100\rangle$ direction as a function of Mg concentration. The solid lines in Figs. 5–7 represent predictions of the rigid-band model discussed in the text using Ashcroft's band-structure masses.

orientation of the magnetic field. The area at an angle θ from the symmetry axis is then given, to lowest order in θ, by

$$\mathbf{A}(\theta)=\pi r_0^2(1+\alpha\theta^2). \tag{6}$$

It now follows that

$$\left|\frac{\partial^2\mathbf{A}}{\partial k_z^2}\right|^{1/2}=(\sqrt{4\pi})\,|\alpha-\tfrac{1}{2}|^{1/2}, \tag{7}$$

and α can be determined by comparing the rotation diagram with that expected for a perfect cylinder, noting that

$$\frac{\mathbf{A}(\theta)-\mathbf{A}(\theta)_{\text{cyl}}}{\mathbf{A}(\theta=0)}=(\alpha-\tfrac{1}{2})\theta^2. \tag{8}$$

When $bT/H<1$, the MTO effect exhibits large harmonic content. It is thus of some interest to compare the harmonic content of the MTO signal from pure Al with that expected from theory. A recording of the pure Al signal arising from the γ oscillations for H near $\langle 110\rangle$ yields a ratio of first harmonic to fundamental amplitude of approximately 0.27; the theoretical value for this ratio at the appropriate temperature and field is 0.185, if we use the measured Dingle temperature of 1.5°K.

B. Aluminum-Magnesium Alloys

1. Size and Shape of Fermi Surface

Frequency and its angular variation were measured in an effort to ascertain changes in size and shape of the third-zone Fermi surface with magnesium concentration. Although data for the alloys was taken throughout the {100} plane, the frequency spectrum could be analyzed most easily near the $\langle 100\rangle$ and $\langle 110\rangle$ directions. This was especially true for the higher-concentration alloys where the signal-to-noise ratio was reduced.

The MTO technique, as we have used it, becomes less sensitive as the frequency of the oscillation diminishes. Consequently, the α oscillations (Fig. 5) were the most difficult to observe. Operation at higher fields, while decreasing the damping due to the Dingle factor, only enhances this effect. The β oscillations (Fig. 6) were of sufficient amplitude to permit observation in an alloy of 0.4 at.% magnesium concentration. These oscillations were resolved most clearly near $\langle 110\rangle$. The β oscillations derive from the bulged junction of the areas near the point W in the Brillouin zone. As this region is particularly sensitive to changes in the band structure relative to the Fermi energy, we might expect that these oscillations will be especially sensitive also to deviations from the RBM approximation. The observed frequency changes are, however, in good agreement with the predictions of the RBM as presented below. It is noteworthy, however, that the angular variation for the β orbits in a {100} plane exhibit a relative maximum at $\langle 100\rangle$ for the most dilute alloys but a weak relative minimum at that direction for the most concentrated alloy sample. This clearly suggests a change in the shape of the Fermi surface in the region near W, but we do not have sufficient data to interpret the changed shape. Further experiments, using higher magnetic fields and a wider range of alloy concentration would be valuable.

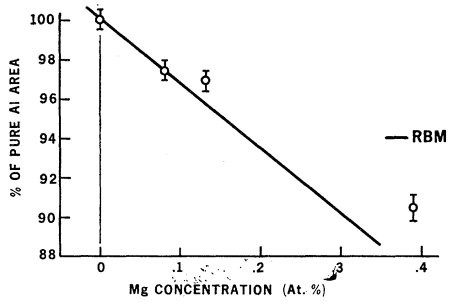

FIG. 6. Changes of the β cross section for the $\langle 110\rangle$ direction. As no band-structure mass was available, we have used the RBM prediction of Ref. 2 in this figure.

The γ oscillations (Fig. 7) were studied extensively in pure Al and in the two most dilute alloy samples. The probable relative error for these measurements is between 0.1 and 0.2 %. The values of α of Eq. (6), as determined from rotation patterns between 0° and 10° from $\langle 100\rangle$ in the manner discussed in Sec. III A, are 0.62, 0.72, and 0.75±0.05 for pure Al and the 0.08 and 0.13%-Mg samples, respectively. As in the case of the β oscillation, there is evidence of a small change in the shape of the Fermi surface, although the $\langle 100\rangle$ frequencies do scale in conformity with the RBM.

The variation in frequency with electron concentration, using the RBM, is given by the following argument. If following Friedel,[10] we assume the effect of the valence difference between solvent and solute is a rigid displacement of the band edge relative to the Fermi energy,

[10] J. Friedel, Advan. Phys. **3**, 446 (1954); Phil. Mag. **43**, 153 (1952).

the effect of alloying on the free-electron Fermi surface can be calculated very simply.[11]

For the Fermi energy and band-edge energy we have

$$E_F \propto (n/V_a)^{2/3}; \quad E_b \propto (1/a)^2; \quad V_a \propto a^3,$$

where n is the electron/atom ratio, V_a is the atomic volume, a is the interatomic distance, and E_b is the energy at the band edge which is assumed to occur at a symmetry point on the Brillouin-zone face. It is now easily shown that

$$\delta E_F - \delta E_b = \tfrac{2}{3} E_F \delta n/n - \tfrac{2}{3}(E_F - E_b)\delta V_a/V_a. \quad (9)$$

In our case, the second term in (9) may be neglected since for the third-zone Fermi surface of Al, $E_F \simeq E_b$ and, moreover, the atomic volume of Al is quite insensitive to small additions of Mg.[12]

Since $m_c^* = (\hbar^2/2\pi)(\partial \mathbf{A}_o/\partial E)_{E_o}$ and $f = \hbar c \mathbf{A}_o/2\pi e$, the frequency shift δf will be given by

$$\delta f = (7.87 \times 10^8)(m_c^*/m)(\delta n/n) E_F, \quad (10)$$

where δf is in gauss and E_F in rydbergs. The RBM predicted changes in frequency (see Figs. 5–7) are based on Eq. (10).

2. Dingle Temperature and Effective Mass

Using the method discussed in Sec. II, we have measured a parameter $m_c^* X_D$. The measurements were

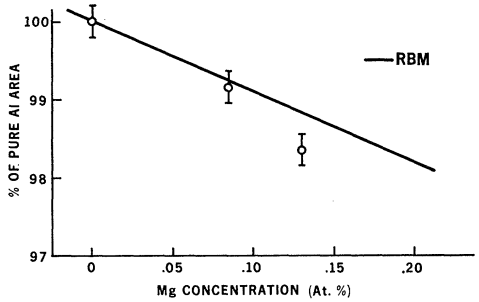

FIG. 7. Changes in the γ cross section for ⟨110⟩ as a function of Mg concentration.

restricted to orientations for which little beating occurred or for which several beat cycles could be observed and the amplitude pattern established with reasonable accuracy. These restrictions eliminated the γ oscillation near ⟨100⟩ from this series of measurements.

To minimize extraneous amplitude variations associated with the detection system, we used no filtering for these measurements. It is worth noting that since we do not employ a field modulation technique the amplitude of our signals are not limited by a field-dependent skin depth nor influenced by changes in effective-modulation amplitude as the field is swept.

TABLE I. Amplitude comparison for ⟨110⟩ data. The damping of the oscillations as predicted by the Dingle theory using the measured Dingle temperatures is compared with the direct measurement. The direct data have been standardized to the pure-aluminum results.

At.% Mg	Approx. freq. G	X_D (°K) (Measured)	Alloy amplitude reduction: Dingle theory	Direct measurement
Pure	5×10^5	0.4	0.65	
	3×10^6	1.5	0.22	
0.08	5×10^5	2.8	0.09	0.08
	3×10^6	2.7	0.02	0.06
0.13	5×10^5	2.5	0.13	0.11
	3×10^6	3.7	0.01	0.02
0.39	5×10^5	4.7	0.02	0.03

The dependence of X_D in alloy concentration is shown in Fig. 8. The solid line shows the effective Dingle temperature calculated from the resistivity, using the relation

$$X_D = \hbar/2\pi k \tau_\rho,$$

where τ_ρ is the resistivity relaxation time ($\tau_\rho = m/ne^2\rho$). Since τ_ρ is a relaxation time averaged over the entire Fermi surface, detailed agreement cannot be expected.

In addition to exhibiting the anticipated increase of X_D with increasing concentration, the data for the γ oscillations show a further enhancement of X_D. This relatively large Dingle temperature probably accounts for our inability to observe the γ oscillations in the most concentrated sample. Priestley[13] has shown that the effect of a random microstructure is to reduce the amplitude of dHvA oscillations by a factor $\exp[-(\pi a b f/H)^2]$, where $a = (1/f)df/d\theta$, b is the Gaussian half-width of the distribution of cross-section areas, and f is the mean frequency. Since the γ oscillations have a higher frequency than the others, the greater reduction of the γ-oscillation amplitudes relative to the β oscillations might be due to such microstructure.

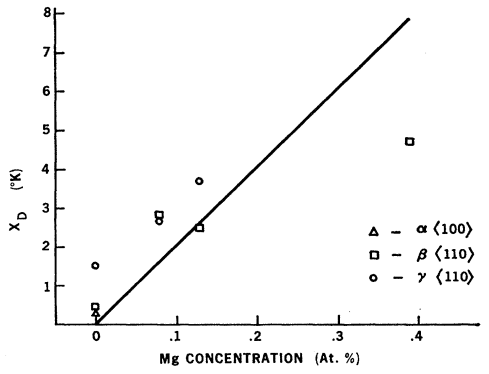

FIG. 8. Variation of the Dingle temperature X_D with alloy concentration. The solid line has been obtained from the resistivity using the free-electron mass.

[11] Although this calculation has been made in SG we have reproduced it here because of obvious errors in SG's footnote 55.

[12] W. B. Pearson, *A Handbook of Lattice Spacings on Structures of Metals and Alloys* (Pergamon Press, Ltd., London, 1958), p. 367.

[13] M. G. Priestley, Phil. Mag. **79**, 1205 (1962).

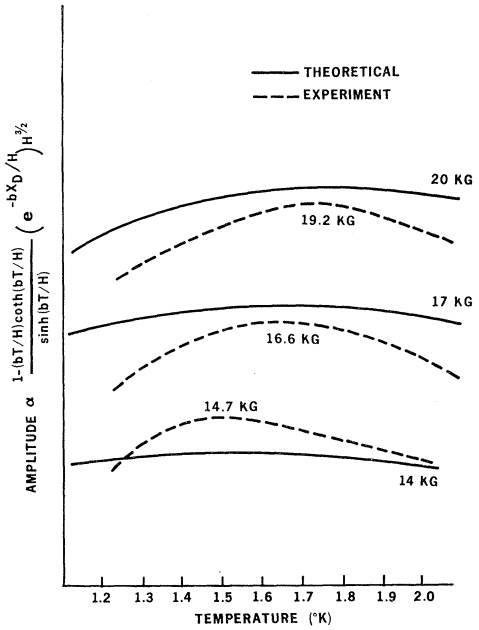

FIG. 9. Amplitude envelope of the MTO data. The theoretically predicted solid curves contain only the fundamental term, i.e., $l=1$.

Table I compares the measured reduction in amplitude with that calculated from the measured Dingle temperatures. The agreement is reasonably good in view of the fact that small errors in X_D result in rather large changes in the damping. The absolute amplitude of the γ oscillations for H along $\langle 110\rangle$ was also measured and compared with the theoretical expression. The two agree within experimental error.

From the amplitude-versus-temperature data we were able to determine the effective mass for the β orbits near $\langle 110\rangle$. The measurements were made over fields ranging from 11.9 to 20.9 kG, and some of our curves of amplitude versus temperature are reproduced in Fig. 9, where we also show the expected theoretical curves. Two features are noteworthy. First, the experimental curves show a more pronounced peak than the theoretical. Second, the effective mass, determined from the value of bH/T at which the amplitude reaches its maximum value, is field dependent, increasing monotonically from about 0.104 to 0.121 m with increasing field.

This field dependence of m_c^* is most suspicious and is, in fact, not real. As we mentioned earlier, we did not use a frequency filter in these measurements and, consequently, the total amplitude of the signal is enhenced by the presence of higher harmonics. These harmonics are particularly pronounced at low temperatures and high fields. Thus, the amplitude maxima are shifted to lower temperatures, and this shift is more pronounced at higher fields. Neglect of the harmonic content therefore leads to the apparent dependence of m_c^* on H, and moreover, accounts for the sharper peaks of the experimental amplitude versus temperature curves. Evidently, in the detailed interpretation of MTO data when $X_D \lesssim 1$, it is important to properly account for the presence of higher harmonics in the observed signals.

ACKNOWLEDGMENT

We are grateful to H. J. Trodahl for his advice and assistance especially in the design of the sweep-control circuit.

APPENDIX

It is often desirable to observe quantum oscillatory phenomena such as the dHvA effect periodically in time, requiring a field sweep for which

$$H(t)=a/(t-t_0). \tag{A1}$$

An important advantage of such a sweep is that it permits electronic filtering of the experimental signal to isolate the oscillations due to a single frequency.

A number of authors have reported circuits for accomplishing Eq. (A1) utilizing mechanically driven potentiometers to obtain a $1/t$ signal.[14,15] There are also a number of schemes for simply obtaining a signal proportional to $1/H$,[15,16] which is convenient for data display on an X-Y recorder, but does not provide the filtering capability discussed above. The circuit we have used produces a $1/t$ field sweep without the use of any external time-controlled reference. Furthermore, the circuit is quite easily adapted for use in any number of sweep forms and has, in fact been, used for the generation of linear ($H \propto t$) and exponential ($H \propto e^{\beta t}$) sweeps as well as the $1/H$ sweep.

The basic circuit is a second-generation model of a sweep control originally designed by J. J. Le Page[17]; a simplified diagram is shown in Fig. 10. A signal proportional to dH/dt, derived from a stationary pickup coil, is compared with a reference supplied externally

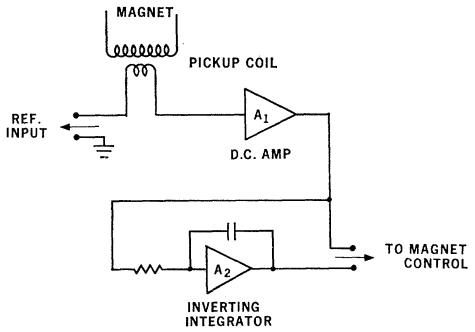

FIG. 10. Sweep-control circuit. Amplifiers A_1 and A_2 are Philbrick P65AU and SP656 amplifiers, respectively.

[14] J. B. Ketterson and Y. Eckstein, Rev. Sci. Instr. **37**, 44 (1966).
[15] A. S. Joseph and W. L. Gordon, Phys. Rev. **126**, 489 (1962).
[16] R. J. Higgins, Rev. Sci. Instr. **36**, 1526 (1965).
[17] J. J. LePage, Ph.D. dissertation, Michigan State University, 1965 (unpublished).

to this section of the circuit. The sweep control attempts to minimize the difference between these two signals by controlling the magnet current. The integrator provides the cumulative sweep signal while the amplifier output (which doubles as the integrator input) is used to eliminate fluctuations with frequency greater than 1 Hz. The circuit as shown requires a floating-reference input to the magnet power supply, which cannot be realized with our Harvey-Wells Model HS-10200 supply. We have overcome this difficulty by isolating the sweep-control circuit from ground.

If a constant reference voltage is supplied to the circuit of Fig. 10, the resulting field sweep is linear in time ($H \propto t$). Such a reference can be built into the sweep-control circuit. Of course, any other sweep form requires a time-dependent reference, although it need not be time controlled.

Assume that the desired sweep is defined by

$$H = F(t) \tag{A2}$$

or, inverting Eq. (A2),

$$t = G(H) = F^{-1}(H). \tag{A3}$$

The reference for such a sweep is

$$\text{Ref} = dH/dt = dF/dt = 1/(dG/dH). \tag{A4}$$

Thus, if one requires that

$$H \propto t^n, \tag{A5}$$

the reference signal must be of the form

$$\text{Ref} \propto t^{n-1} \propto H^{(n-1)/n} \tag{A6}$$

A reference signal proportional to the field raised to any power can be derived from a linear field measuring device (e.g., a rotating coil or Hall device) using a log-amplifier-antilog circuit of standard design.[18,19]

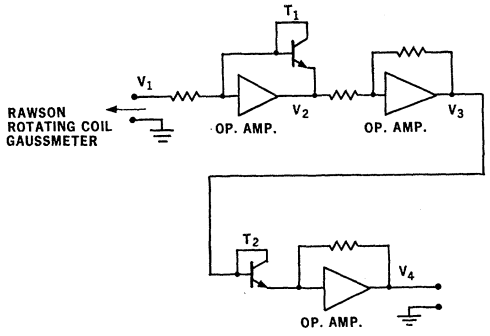

FIG. 11. Squaring circuit used with the sweep control. All amplifiers are Philbrick P65AU operational amplifiers. If the circuit is correctly biased, $V_2 \propto \ln V_1 = V_3 = 2V_2$, $V_4 \propto \exp V_3 \propto V_1^2$. T_1 and T_2 are 2N-299 and SK-3004 transistors, respectively.

The exponent n for a $1/t$ sweep is -1, so that the required reference is

$$\text{Ref} \propto H^2. \tag{A7}$$

A simplified diagram of the circuit used to obtain this reference voltage is shown in Fig. 11. The transistors that we use are not necessarily the best choices, for we are able to obtain accurate (1%) squaring over little more than one decade at the output. Figure 4 above shows data taken using this system.

It follows from Eq. (A4) that the reference signal needed for an exponential field sweep (i.e., $H \propto e^{\beta t}$) must be proportional to H.

The circuits in use in our laboratory are more complex in detail than those shown in Figs. 10 and 11. Most of the added complexity arises from requirements of versatility, convenience, and, in the case of the squarer, component adjustment.

[18] William L. Paterson, Rev. Sci. Instr. **34**, 1311 (1963).
[19] Applications Manual for Computing Amplifiers, George A. Philbrick Research, Inc., 1966 (unpublished).